CONF-950963--7

Proceedings, 8th International Conference on Coal Science to be held in Oviedo, Spain on September 10-15, 1995.

STRUCTURAL ELUCIDATION OF ARGONNE PREMIUM COALS: MOLECULAR WEIGHTS, HETEROATOM DISTRIBUTIONS AND LINKAGES BETWEEN CLUSTERS*

Randall E. Winans, Yeonhee Kim,
Jerry E. Hunt and Robert L. McBeth

Chemistry Division
Argonne National Laboratory
9700 So. Cass Avenue
Argonne, IL 60439

*This work was performed under the auspices of the Office of Basic Energy Sciences, Division of Chemical Sciences, U.S. Department of Energy, under contract number W-31-109-ENG-38.

Structural Elucidation of Argonne Premium Coals: Molecular Weights, Heteroatom Distributions and Linkages Between Clusters

Randall E. Winans, Yeonhee Kim, Jerry E. Hunt, and Robert L. McBeth

Chemistry Division, Argonne National Laboratory, 9700 S. Cass Avenue, Argonne, IL 60439 USA

1. INTRODUCTION

The objective of this study is to create a statistically accurate picture of important structural features for a group of coals representing a broad rank range. Mass spectrometric techniques are used to study coals, coal extracts and chemically modified coals and extracts. Laser desorption mass spectrometry is used to determine molecular weight distributions. Desorption chemical ionization high resolution mass spectrometry provides detailed molecular information on compound classes and carbon number distribution. Structural information on important classes of molecules is obtained using tandem mass spectrometry. These results are correlated with other direct studies on these samples such as solid NMR, XPS and X-ray absorption spectroscopy. From the complex sets of data, several general trends are emerging especially for heteroatom containing species.

From a statistical point of view, heteroatoms must play important roles in the reactivity of all coals. Direct characterization of sulfur containing species in the Argonne coals has been reported from XANES [1,2] and XPS [1] analysis. Indirect methods used include: TG-FTIR [3] and HRMS [4] which rely on thermal desorption and pyrolysis to vaporize the samples. Both XANES [5] and XPS [6] data on nitrogen has been reported, but at this time, the XPS information is probably more reliable. Results from HRMS will be discussed in this paper. Most other information on nitrogen is limited to analysis of liquefaction products. However, nitrogen can be important in influencing characteristics of coal liquids and as a source of NO_x's in coal combustion.

The size of the stable aromatic clusters in coals have been determined for whole coals and pyridine extracts by NMR [7]. The values reported are compatible with those determined by FIMS [8], HRMS [4] and LDMS [9]. All of these techniques give values that are not very large; most species have molecular weights of less than 1000.

2. EXPERIMENTAL

A complete description of the coal samples has been published [10]. Preparation of the extracts and their characteristics have been described [11]. Desorption high resolution mass spectra were taken on a 3-sector MS-50 either in electron impact or chemical ionization mode. Samples were heated in the source from 200 to 700 °C at 200 °C/min. A Diels-Alder adduct of maleic anhydride and perdeutero anthracene is used as an internal standard. Precise mass measurements are averaged from scans over the entire temperature range. Formulas are assigned and the data sorted via a procedure developed in this program. Only formulas that fit within ± 3.5 millimass units are considered.

3. RESULTS AND DISCUSSIONS

High resolution mass spectrometry data can be sorted by both heteroatom content and by hydrogen deficiency which is also termed double bond equivalents and is related to z-number. From hydrogen deficiency, the size of aromatic clusters can be estimated. The variable with rank in cluster size for molecules containing either oxygen, sulfur or nitrogen is shown in Figure 1. Since oxygen is the most abundant heteroatom, most of the multiple species contain at least one oxygen. Therefore, this heteroatom data was sorted into three categories (1) molecules which contain only oxygen; (2) molecules with at least one sulfur; and (3) molecules with at least one nitrogen.

For oxygen functionalized molecules, the cluster size increases smoothly with increasing rank. The nature of the oxygen species also changes with rank. The low rank coals contain between 20-30% of oxygen in ethers or furans, small amounts of carboxylic acids and the rest are aryl hydroxy compounds. Aliphatic ethers are only found in the lignite and subbituminous coal samples. In the highest rank coal, lv bituminous (APCS 5), over 90% of the oxygen is found as furans and possibly ethers. NMR, methylation, and HRMS all give essentially the same result for this coal.

Sulfur, of all the heteroatoms, has the greatest amount of the aliphatic forms. The average value of aliphatic sulfur for each of the Argonne coals from a number of techniques is shown in Figure 2. There is a surprisingly large amount of aliphatic sulfur in the lower rank coals and there appears to be a smooth decrease with rank. Prominent aliphatic compounds observed by HRMS include:

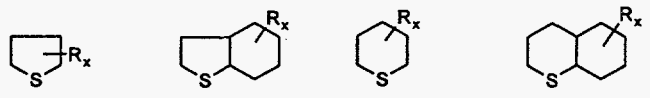

These classes of compounds have been seen in sediments [12]. This aliphatic sulfur should be easy to remove but also will thermally convert to the more stable thiophenes. The size of the clusters increase with increasing rank in a similar manner to the oxygen species, but tend to be smaller overall.

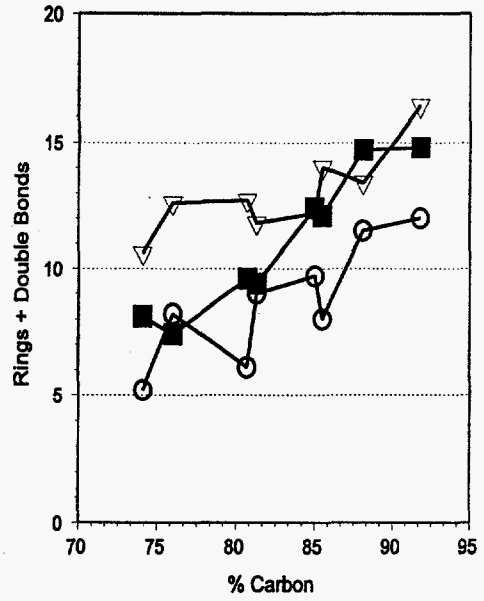

Figure 1. Size of aromatic clusters determined from DEIHRMS. ■ O_1, O_2, O_3, O_4; ○ S, S_2, SO, SO_2; ▽ N, N_2, NO.

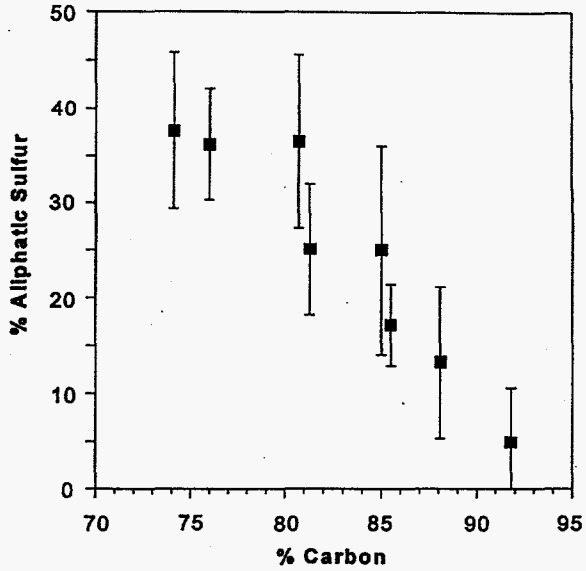

Figure 2. Averaged values for aliphatic sulfur from XANES [1,2], XPS [1], HRMS [4], and TG-FTIR [3].

The nitrogen containing molecules are very different. Data from XPS [6] and mass spectrometry show that pyrrole and pyridine types dominate, assuming that quaternary nitrogen seen in XPS is pyridine. As seen in Figure 3, the distribution of these types are independent of rank. There is a close correlation for pyridine nitrogen between XPS and HRMS.

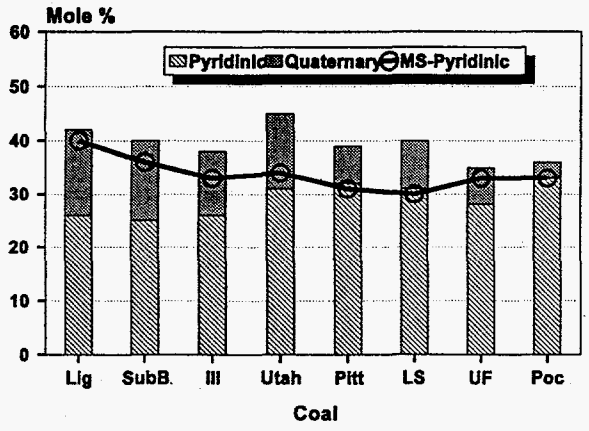

Figure 3. Nitrogen group analyses comparing XPS and HRMS results.

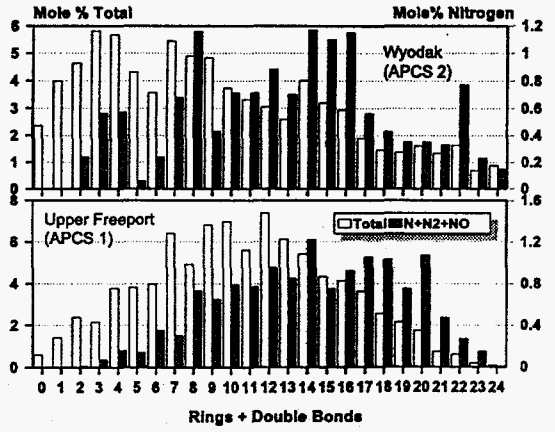

Figure 4. The distribution of molecular clusters with nitrogen compared to all molecular clusters.

What is even more striking is that the cluster size does not vary substantially with rank (Figure 1). For example, the distribution for the Wyodak subbituminous coal and the Upper Freeport are quite similar as is shown in Figure 4. The formation of these molecules must occur very easily in the coalification process. Note that no amines have been observed.

4. CONCLUSIONS

Aliphatic sulfur is found in all ranks of these coals, while aliphatic oxygen is only observed by HRMS in the lowest rank coals. For oxygen and sulfur, heteroatom cluster size increases with rank. Surprisingly, the cluster size of nitrogen compounds is only slightly rank dependent and the forms of nitrogen is also rank independent. No amines are observed by HRMS.

ACKNOWLEDGMENTS

This work was performed under the auspices of the Office of Basic Energy Sciences, Division of Chemical Sciences, U.S. Department of Energy, under contract number W-31-109-ENG-38.

REFERENCES

1. G. N. George, M. L. Gorbaty, S. R. Kelemen, and M. Sansone, Energy Fuels, 5 (1991) 93.
2. G. P. Huffman, S. Mitra, F. E. Huggins, N. Shah, S. Vaidya, and F. Lu, Energy Fuels, 5 (1991) 574.
3. R. Bassilakis, Y. Zhao, P. R. Solomon, and M. A. Serio, Energy Fuels, 7 (1993) 710.
4. R. E. Winans, "Mass Spectrometric Studies of Coals and Coal Macerals," in Advances in Coal Spectroscopy, H. L. C. Meuzelaar (ed.), Plenum Press, New York, 1992, 255.
5. S. Mitra-Kirtley, O. C. Mullins, J. Branthaver, J. Van Elp, and S. P. Cramer, Preprint, Div. Fuel Chem., ACS, 38 (1993) 756.
6. S. R. Kelemen, M. L. Gorbaty, and P. J. Kwiatek, Energy Fuels, 8 (1994) 896.
7. T. H. Fletcher, S. Bai, R. J. Pugmire, M. S. Solum, S. Wood, and D. M. Grant, Energy Fuels, 7 (1993) 734.
8. N. Simmleit, H.-R. Schulten, Y. Yan, and H. L. C. Meuzelaar, "Thermochemical Analysis of U.S. Argonne Premium Coal Samples by Time-Resolved Pyrolysis FIMS," in Advances in Coal Spectroscopy, H. L. C. Meuzelaar (ed.), Plenum Press, New York, 1992, 295.
9. J. E. Hunt and R. E. Winans (this volume).
10. K. S. Vorres, Energy Fuels, 4 (1990) 420.
11. R. E. Winans, R. L. McBeth, P. E. Melnikov, and R. E. Botto, Proceedings, 1993 International Conference on Coal Science (1993) 515.
12. H. L. ten Haven, J. Rullkötter, J. S. Sinninghe Damsté, and J. W. de Leeuw, "Distribution of Organic Sulfur Compounds in Mesozoic and Cenozoic Sediments from Atlantic and Pacific Oceans and the Gulf of California," in Geochem. of Sulfur in Fosil Fuels, W. L. Orr and C. M. White (eds.), ACS Symp. Series 429 (1990) 613.

2.1 Output Energy and Stability

Figure 1 is a schematic diagram of the singly resonant OPO architecture, and figure 2 is the optical layout of the experimental testbed used to collect data pertinent to the OPO performance. Figure 3 shows the OPO conversion efficiency using this pump source for both a flat-flat cavity and a hemispherical cavity. The data in Fig. 3 exhibits a strong energy balance anomaly for the hemispherical cavity. Ideally, the ratio of idler to signal energies should be inversely proportional to the ratio of the their wavelengths ($\cong$ 0.45). For the flat-flat configuration, this ratio was very close to ideal, but for the hemispherical cavity this ratio was only about 0.25, indicating that either mid-IR idler energy may have been diffracted, scattered, or absorbed in route to the energy head, or that signal energy measurements were not accurate. We reason that the former option is the most likely since the signal energy measurements for the hemispherical and flat-flat cavities are very close and the flat-flat cavity energy balance ratio was within experimental uncertainty. Figure 4 shows the observed buildup time for the signal wave using the hemispherical cavity. It is clear that a longer, flatter pulse at the same peak drive would convert more efficiently. In both cavities, the conversion efficiency was primarily limited by buildup time and dynamic range effects[1].

In theory, the shot-to-shot energy stability of the OPO output should not affect the accuracy of the DIAL measurement because the DIAL return signals are normalized to the output pulse energies, but in practice, increased energy stability reduces the demands for dynamic range and linearity on the detector and associated electronics. The energy stability of the mid-IR output was the same for both cavity configurations. For these experiments, the pump pulse energy was steady to within 1% (RMS) of the mean. The injection seeded OPO output was stable to better than 2% (RMS) of the mean when pumped well above (2x) the threshold energy. As the pump energy decreases towards oscillation threshold, the stability of the OPO decreases.

2.2 Frequency Locking and Stability

As seen in Fig. 1, there were no line narrowing components included in the OPO cavity itself. Two factors ensured the single frequency character of the mid-IR idler output. First, the pump source was single frequency, and second, the cavity length was actively controlled to be resonant with the wavelength of the OPO injection-seed laser.

The seed beam was expanded and collimated by the use of a shear plate before injection into the OPO cavity. We found that it was strongly astigmatic, as is typical for beams emitted from polarization preserving fiber optics. Figure 5 shows the degree of astigmatism of the seed beam. The average power of the seed light which was delivered to the OPO was typically a few tenths of a milliwatt.

It was found that the increase in output energy, or better, the increase in brightness of the OPO output when seeded could serve as a reasonable locking signature. However, the increase in output energy was small when the OPO was operated well above threshold (e.g. see Fig. 3), so the success of this scheme depended on having a very stable pump source. The increase in brightness was, in general, a more distinct locking signature than the increase in energy alone. Figure 6 shows the change in the far field profile of the idler beam when it was seeded. It was assumed that the signal beam divergence also diminished when seeded. In practice, the signal energy which leaked through the rear cavity mirror was measured after it was focused through a pinhole aperture, and the locking software moved the cavity length to maximize this signal. Although it was generally a higher contrast signature than the energy alone, this locking signal was susceptible to both drifts in pump irradiance profile and OPO alignment which could steer the signal beam.

The algorithm for cavity locking was as follows: Initially the cavity length (PZT voltage) was scanned over one free spectral range to find a position where the energy (brightness) was a maximum. Typically the FWHM of the brightness signature was $\cong$ 20% of the cavity free spectral range. The PZT was then sent to that position where the maximum was found. Subsequently, the PZT did a 3 point dither about that

position. At each of the three positions, the energy (brightness) was measured and the new PZT position was chosen to be the one with the largest signal. The dither procedure was repeated every few seconds.

To check how closely the algorithm was tracking the optimal length for resonance with the injection seeder, we recorded data for a one hour period during which every 60 seconds the PZT was scanned over a range approximately three times the FWHM of the locking signature, and the position of maximum energy (brightness) was determined. The difference between the last PZT position before the scan and the position of the maximum found during the scan was taken as a measure of how far from the true maximum the cavity length was at the time the scan was initiated. This difference in cavity length δL corresponded to a deviation of the cavity resonant frequency from the injection-seeder frequency $\delta\nu$ given by:

$$\delta\nu = 2FSR(\delta L/\lambda) \qquad (1)$$

where FSR is the cavity free spectral range and λ is the injection-seeder wavelength. Figure 7 is a plot of the apparent frequency stability derived from this scanning procedure, done over an hour period.

2.3 Spatial and Angular Characteristics

Although the mid-IR energy output of the hemispherical cavity was measured to be less than that of the flat-flat cavity, the improved spatial and angular characteristics of the mid-IR beam made this cavity configuration more attractive for our application. Figure 8 is a spatial beam profile of the incident pump beam at the OPO crystal. Figures 9 shows the spatial profile, at the focus of a 500 mm lens, of the idler beam for the injection-seeded flat-flat cavity and the hemispherical cavity. From Fig 9, it is evident that the stable hemispherical cavity produced a much less divergent beam. In the near field, the stable cavity produced a beam that looked essentially gaussian, whereas the critically stable flat-

flat cavity produced a beam that appeared to have constantly changing stripes of varying irradiance throughout the beam profile. When the injection-seeder beam was blocked, these stripes disappeared, thus leading us to believe that they are an interference related phenomena. Unfortunately, accurate data were not recorded that would allow a good quantitative estimate of the idler beam divergence using the commercial pump laser and testbed OPO. However, in the field, idler energy from the hemispherical cavity was focused through a pin hole and the transmission through the pinhole was measured. This measurement indicated that the divergence of the idler beam emitted from the OPO was no worse than five times the calculated diffraction limit.

2.4 Spectral Purity

One of the key issues for DIAL sources is spectral purity. During the course of the OPO testbed experiments, we made several observations regarding the conditions for producing spectrally pure light from the OPO. We observed that the spectral purity was poor when the seed beam was not well collimated and overlapped with the cavity mode. In this case, the unseeded portion of the beam, which contained the spectral impurities, was more angularly divergent than the seeded part, and angular filtering could be used to improve the spectral purity. Figure 10 shows the effect of spatial filtering on both the angular and spectral profile of the idler under these conditions.

The seeder alignment was generally optimized when the unseeded and seeded far field spots were well overlapped. When this was not the case, the seed beam pulled the far field profile over to the angle of the seed beam. When the seeder was well aligned and collimated we still observed some spectral impurities, but had less success improving the spectral purity by spatial (angular) filtering. The most persistent spectral impurities appear to be associated with strong clusters in the unseeded spectrum. These clusters are evidently caused by residual reflectivities at the idler wavelengths on the crystal faces, which modulate the regenerative gain as is found in doubly resonant oscillators (DROs).

Figure 11 shows the effect of seeding a spectrum which showed strong DRO type clusters separated by about 20 GHz. (The spectrometer dispersion was calibrated by using an isotopic doublet at 2775 cm^{-1}. It was determined that in this spectral region, the 128 pixel camera image spanned 205 GHz , i.e.1.6 GHz/pixel, and the spectrometer resolution appeared to be about 4 pixels (6 GHz) FWHM.) By careful alignment of the OPO cavity and seeder beam, and by working with a high enough crystal angle to suppress the DRO effects, a spectral purity of 20:1 or better was observed on the spectrograph during the testbed experiments.

3. OPO FIELD PERFORMANCE WITH 180 HZ THREE-WAVELENGTH PUMP

As stated in the introduction, the testbed experiments were performed with a commercial pump laser that had a near field spatial profile like that shown in Fig. 8. The pump system used for field experiments was developed at LLNL within the Laser Science and Technology Group. The details of this system will not be presented here, but a brief overview of the system is necessary. A photograph of the field test OPO hardware is presented, and data are presented that are pertinent to the energy stability and spectral purity of the OPO when pumped by the 180 Hz system. In addition, results of numerical simulations are shown that agree with observed phenomena occuring when two simultaneous wavelengths were used to pump the OPO. Finally, two DIAL measurement results are shown that exemplify the utility of the multiwavelength pump/OPO source.

3.1 Pump Laser Operating With Three Sequential Wavelengths at 180 Hz

The fielded pump laser was a diode pumped MOPA capable of sequentially emitting three arbitrary single frequency longitudinal modes lying under the gain bandwidth of Nd:YAG. Under the right environmental controls, this system was capable of repeating the pattern of three sequential wavelengths with a shot-to-shot repetition rate of 180 Hz (60 Hz rate for a complete set of three wavelengths) for an indefinite period. The pulse

energy was ≅ 100 mJ and the beam size was adjusted such that 86 % of the total energy was encircled by a diameter of 7.0 mm.

To obtain three wavelength operation at this repetition rate, the use of three single frequency injection-seed lasers and a combination of liquid crystal light valves was used to sequentially seed the master oscillator and thus produce the multi-wavelength operation. The method by which the cavity length was controlled and the injection-seed lasers tuned was essentially the same as reported by Raymond and Smith[2].

By synchronizing the triggers to the liquid crystal light valves with the data acquisition system, the sequence of three wavelengths was clocked with respect to time and the on and off resonance wavelengths for the DIAL measurements were thus identified.

3.2 OPO Hardware Used in the Field

Figure 12 is a close up photograph of the OPO cavity structure. The central optic at 45° to the camera viewing angle is the pump beam input coupler; for scale this optic is one inch in diameter. As seen in Fig. 12, the concave high reflector is to the left of the input coupler, the crystal and it's associated temperature control hardware to the right of the input coupler, the output coupler and PZT stack are to the extreme right of the cavity.

To reduce the demands on the cavity locking algorithm, the rods for the frame of the OPO were constructed from a carbon fiber composite with zero coefficient of thermal expansion. The frame was kinematically mounted on an aluminum base plate. By disconnecting the two twisted pairs (phone plugs) leading to the actuators on each end of the cavity, the OPO frame could be easily removed without disturbing the alignment of the input coupler or the crystal.

The temperature of the crystal was controlled to within ± 0.1°C using thermo-electric cooling elements that pumped heat to or from the crystal using water cooled copper blocks as source or sink elements. The tubing to the water cooled copper blocks is clearly visible in Fig. 12. A white ceramic cover over the perimeter of the entrance face of the

crystal was used to keep diffracted or scattered pump light from heating the copper crystal mount. Temperature control of the $LiNbO_3$ crystal was critical for DIAL measurements on narrow line species because at our wavelength and crystal temperature $d\lambda/dT$ is approximately 160 GHz/°C.

The OPO base plate was bolted to a thermally controlled breadboard that served a dual purpose. The breadboard was used both as a mounting surface for beam steering optics and to provide a large thermal mass to help damp out rapid temperature fluctuations caused by the cycling of the air conditioning units in the field test trailer. The breadboard temperature was controlled by recirculated water pumped through copper tubing imbedded in the breadboard. The breadboard layout is shown in figure 13, and a photograph of the entire OPO system (with thermal enclosure removed) is shown in figure 14.

The OPO system was further protected from rapid temperature fluctuations by a lightweight themally insulating enclosure which dropped over the entire system. The enclosure was built from twin-walled polycarbonate material and provided low pass damping of the temperature fluctuations in the trailer down to a period of about 20 minutes.

3.3 OPO Stability and Spectral Purity

In the field, the idler pulse energies out of the OPO were typically between 0.5 and 1.0 millijoules / pulse. The stability of the OPO idler energy was less than that demonstrated in the testbed experiments primarily because the OPO was operating nearer threshold. Figure 15 is a typical plot of OPO idler energies for a run of 12096 shots. We saw no detrimental effects to OPO performance, from the 18 Watts of average power in this pump beam.

With the 180 Hz pump, the OPO operated at less than 1.25 times above threshold so that the cavity locking algorithm could simply use the increase in idler pulse energy as feedback. This preempted using the spatially filtered signal beam leaking through the high reflector of the cavity as described in section 2.2. Additional work on the alignment and

collimation of the injection-seed laser resulted in excellent spectral purity on all three operating wavelengths as witnessed by the spectrograph output shown in figure 16.

Fig. 16 is showing the image of the entrance slit of a 1 meter spectrometer, as viewed at the plane of the exit slit, integrated over a period of 1/60 of one second. The plane of the exit slit is further imaged on to an InSb focal plane array supported by an industrial PC type computer. The entrance slit is being illuminated with idler light split from the output of the OPO and transported to the spectrometer with an infrared fiber. The spectrometer is the instrument limiting the resolution in this image. Unfortunately, the spectral purity data to be gleaned from this image is only qualitative since the dynamic range and absolute detection limits of the InSb focal plane array were not carefully calibrated against a known blackbody source.

One interesting observation during the field test supported the results of previous numerical simulations. We had predicted that the injection of multiple pumps into an SRO can lead to degraded spectral purity if the frequency separation of the input fields is near a multiple of the cavity resonance of the injected signal wave. In this arrangement, the additional signal frequencies which are generated from the matrix of three-wave interactions will also be resonant with the SRO cavity, leading to poor discrimination of the output fields. Figure 17 shows the results of numerical simulation using a separation between pump wavlengths of six times the FSR of the OPO cavity (FSR ≅ 1 GHz). Figure 18 shows a still frame extracted from video tape of the spectrograph output recorded during operation in the field. Multiple frequencies separated by a $\Delta\nu$ corresponding to the frequency difference between λ_1 and λ_2 are clearly present in Fig. 18.

To illustrate the utility of such a source for mid-infrared DIAL, field test experiments were performed at a standoff of 3.3 Km. Figure 19 shows the result of a DIAL measurement utilizing the OPO source to detect the release of HCl which has a narrow (0.07 cm^{-1} FWHM) absorption peak. For this measurement the absorption is centered at 2925 cm^{-1}.

Figure 20 is an example of the detection of Butanol which has a very broad absorption (300 cm^{-1}). Using the line separation between λ_1 and λ_3 of 22 GHz (see Fig. 16) the stability of the source and detection system was sufficient to sense the differential absorption of λ_1 and λ_3. For this measurement, the central wavelength (λ_2) was tuned to 2971 cm^{-1}.

4. CONCLUDING REMARKS

We have developed a prototype OPO DIAL source that produces a spectrally pure conversion of a Nd:YAG pump laser producing a repetitive series of three sequential wavelengths. The utility of this source for DIAL measurements has been demonstrated by the detection of HCl and Butanol. Further improvements to the system will focus on obtaining a more rapidly tunable system, higher conversion efficiency to the mid-IR, turn key operation and tuning, reduced system size and power consumption, and better quantitative measurements of the spectral purity and frequency stability.

REFERENCES

1. S.P. Velsko and M.S. Webb, "High Average Power Parametric Frequency Conversion - New Concepts and New Pump Sources," *Nonlinear Optics for High-Speed Electronics and Optical Frequency Conversion,* Peygambarian, Everitt, Eckardt, and Lowenthal, Ed., Vol. 2145, pp: 309-315, SPIE Proceedings, Los Angeles, CA, 1994.
2. T.D. Raymond and A.V. Smith, "Two-Frequency Injection-Seeded Nd:YAG Laser," IEEE Journ. Quant. Electron., Vol. 31, No. 10, pp: 1734-1737, 1995.

This work was performed under the auspices of the U.S. Department of Energy by Lawrence Livermore National Laboratory under contract W-7405-Eng-48.

ACKNOWLEDGMENTS

The demonstration of the OPO in the field required a paramount effort on the part of several individuals involved in the design and implementation of the entire remote sensing system. Individual contributions from the following are greatly appreciated:

Detection Group - Asher Blum, Richard Wyeth, David Johnson, Mario Montoya

Laser Group - Brian Comasky, John Halpin, Bryan Moran

Facilities & Coordination - John Weir, James Nally, Robert Guyton

FIGURE CAPTIONS

Figure 1. Singly resonant OPO cavity configuration.

Figure 2. Optical layout for OPO testbed experiments.

Figure 3. Output pulse energy for signal and idler wavelengths as function of pump pulse energy for injection seeded and unseeded operation. (a) flat output coupler and flat high reflector. (b) flat output coupler and 10 meter concave high reflector.

Figure 4. Temporal profile of three pulses pertinent to OPO operation. Hemispherical cavity with CW injection seeding.

Figure 5. OPO injection-seed beam at the focus of +250 mm focal length plano-convex lens. Astigmatic output is typical of single mode polarization preserving fibers. Fiber is rotated 45° for maximum transmittance through faraday isolator.

Figure 6. Spatial profile of idler beam at focus of +500 mm plano-convex lens for both injection-seeded and unseeded operation using the flat-flat cavity. The on axis brightness of the beam is greatly increased by injection-seeding.

Figure 7. Stability of OPO frequency locking algorithm derived from motion of PZT stack used to control cavity length.

Figure 8. Spatial profile of pump beam used for OPO testbed experiments as seen at input face of OPO crystal. Pump laser was a commercial, injection-seeded, 10 Hz, Nd:YAG.

Figure 9. Spatial profile of mid-IR idler beam at focus of +500 mm plano-convex lens.

Figure 10. Effect of spatial filtering on spectral and spatial profile of mid-IR OPO output.

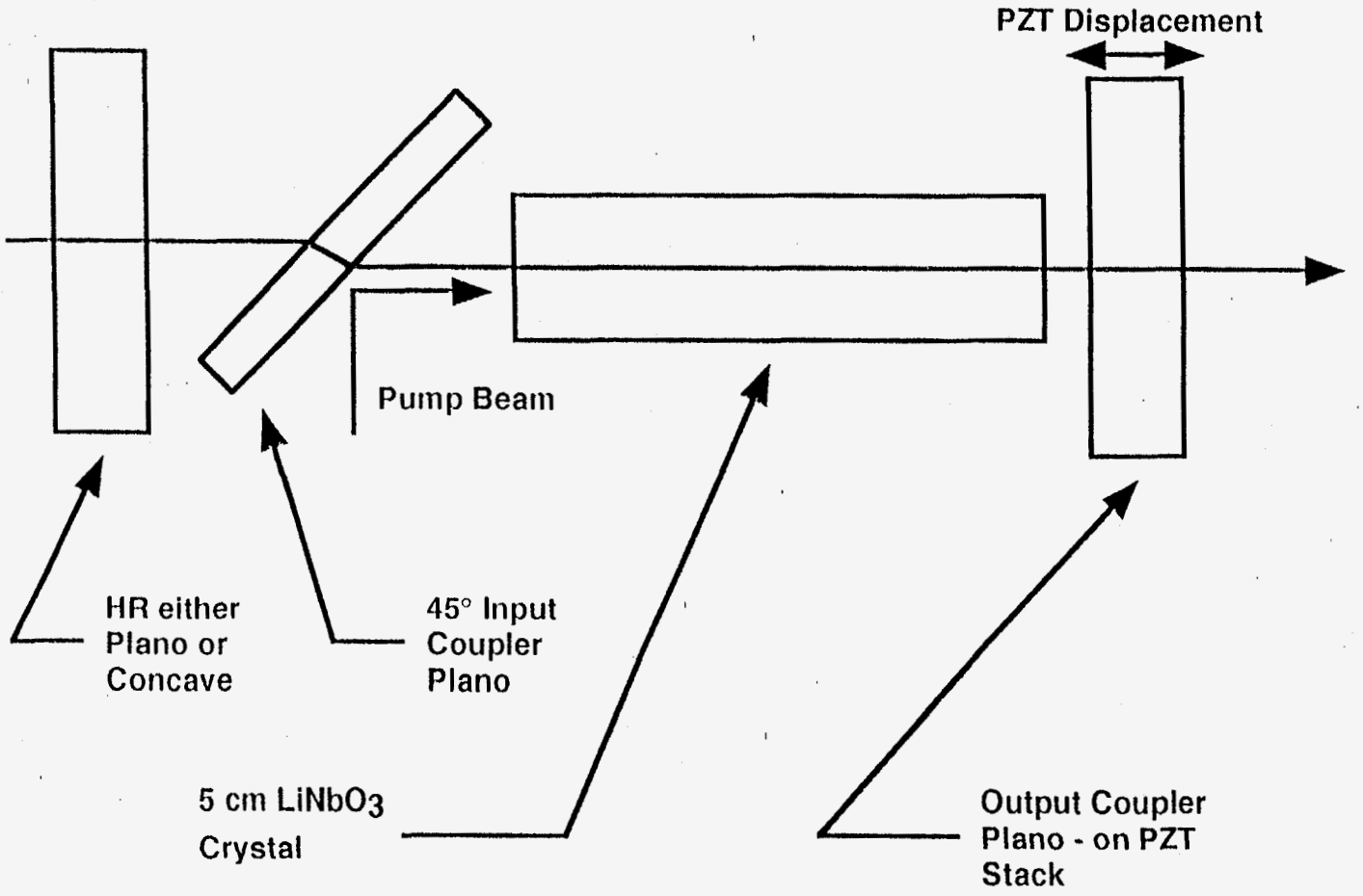

Figure 1 / Webb

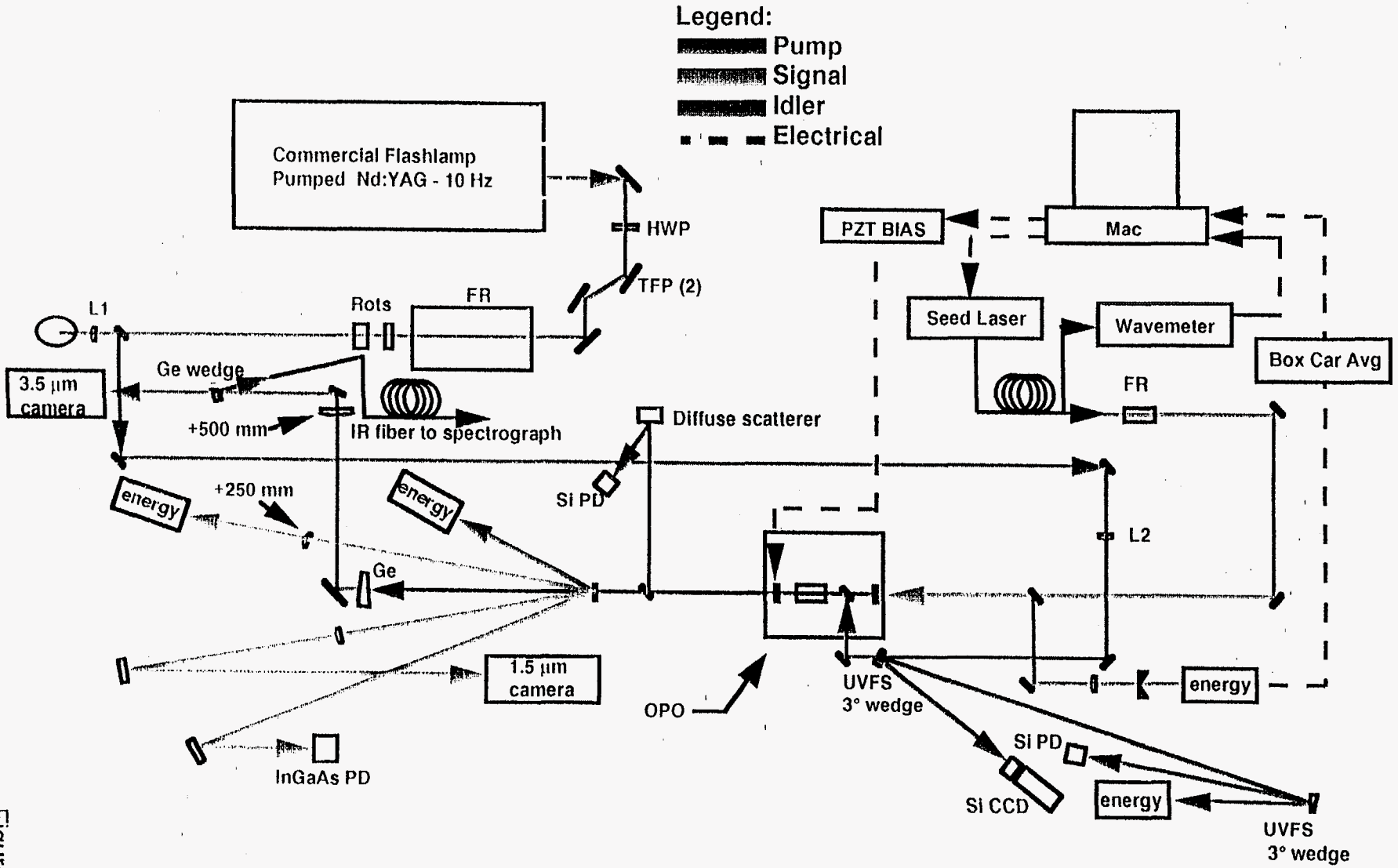

Figure 2 / Webb

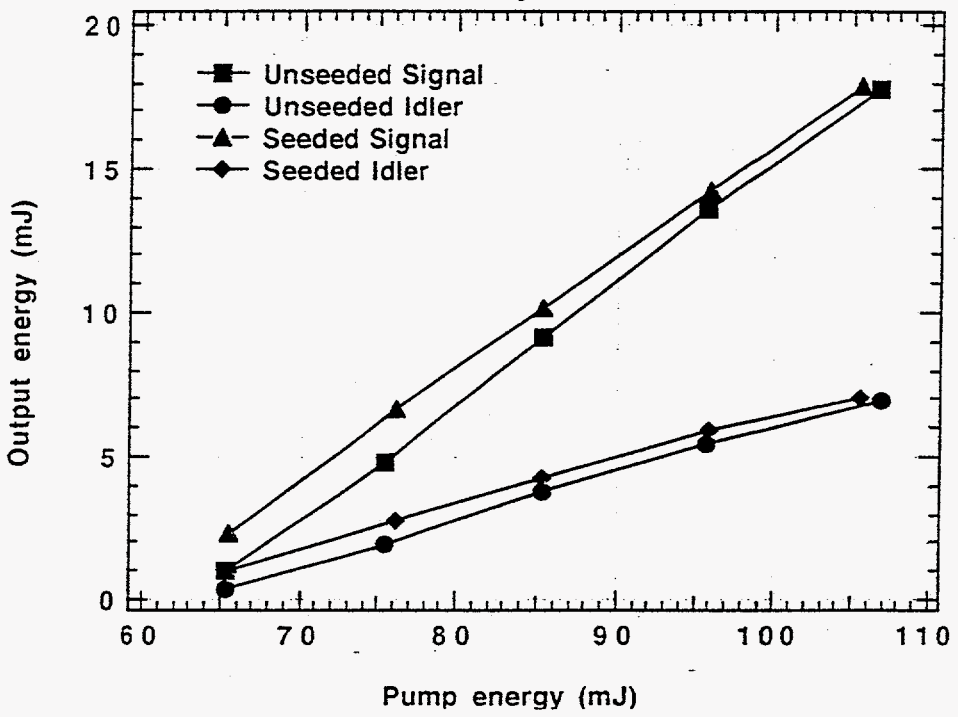

(a)

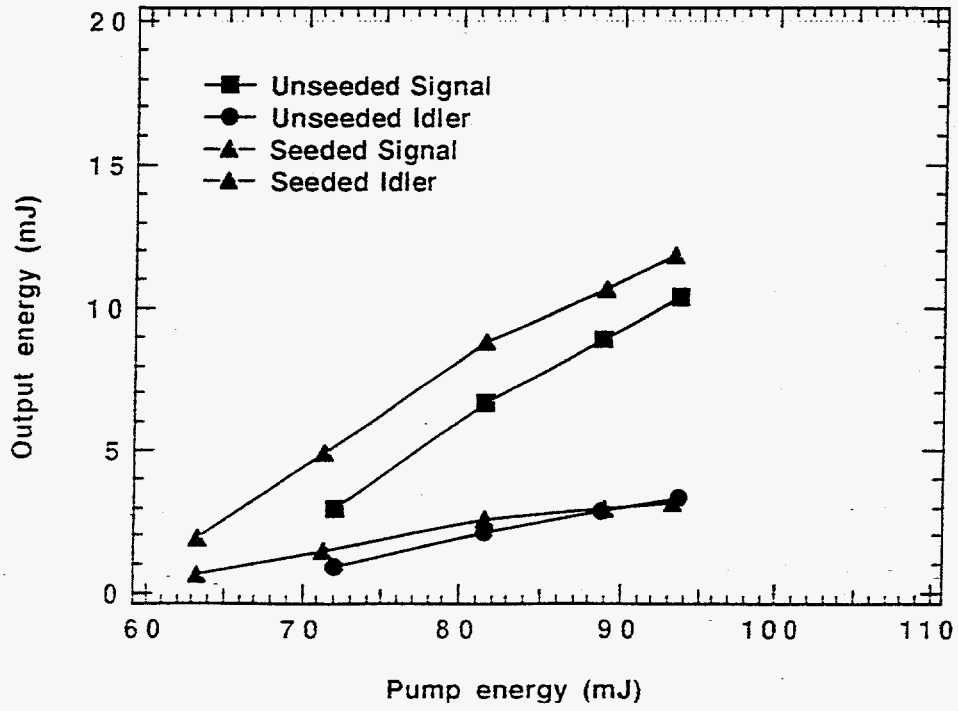

(b)

Figure 3 / Webb

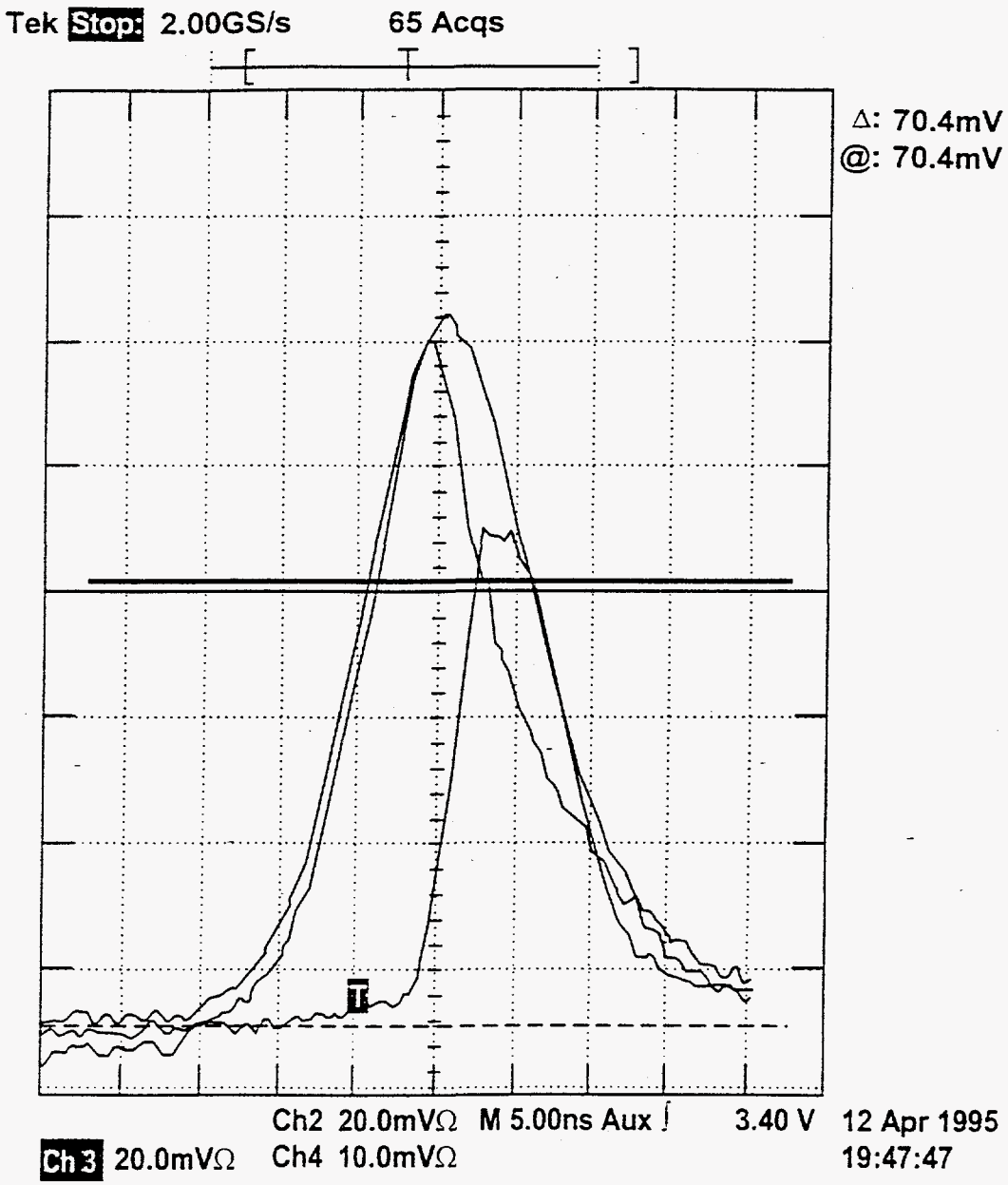

Figure 4/Webb

Seed
Before
Focus

Seed
At
Focus

Seed
After
Focus

Figure 5 / Webb

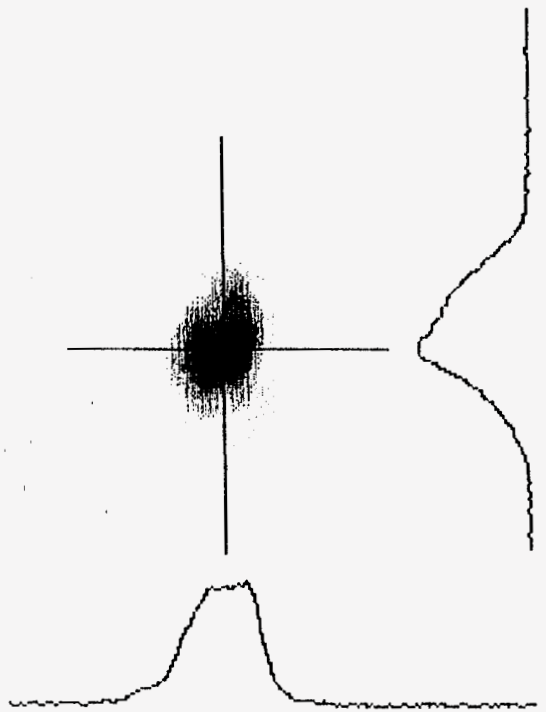

Seeded Idler Profile
at focus of 500 mm lens.

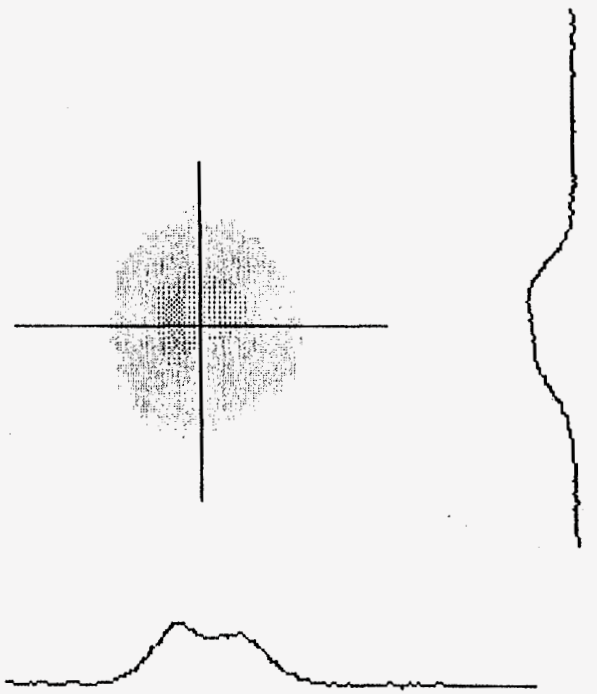

Unseeded Idler Profile
at focus of 500 mm lens.

Figure 6 / Webb

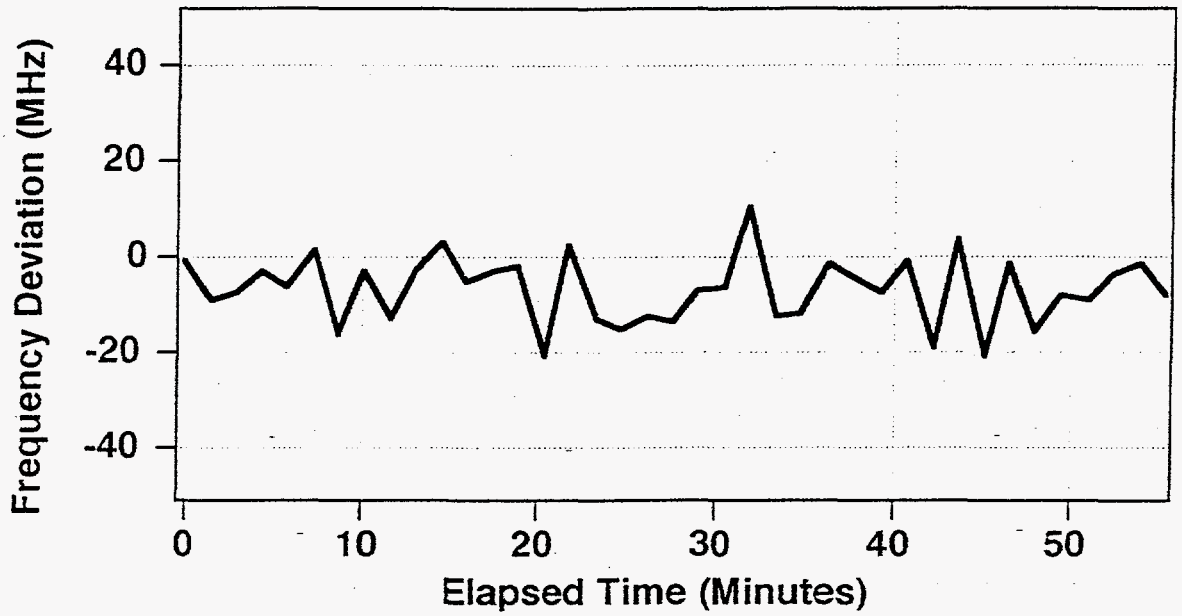

Figure 7 / Webb

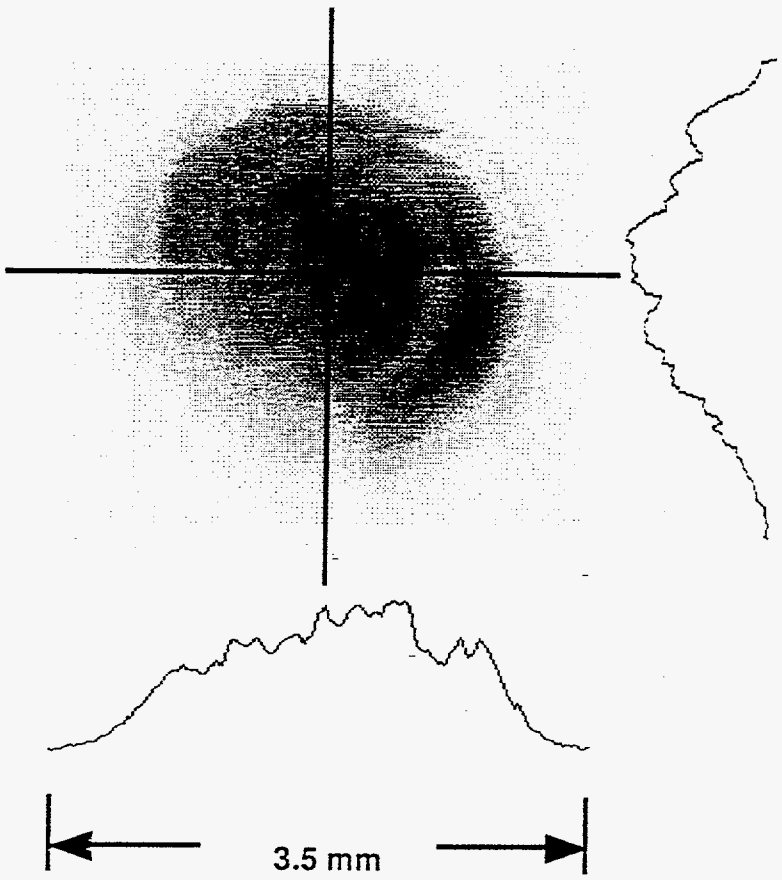

Figure 8 / Webb

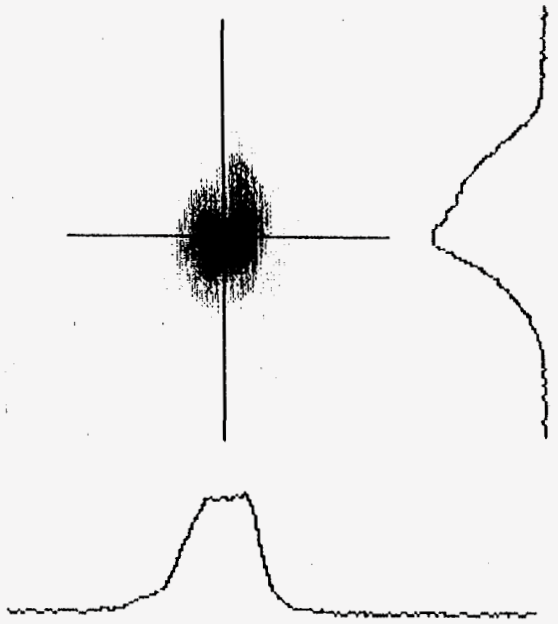

Seeded idler profile
at focus of 500 mm lens
for flat - flat cavity.

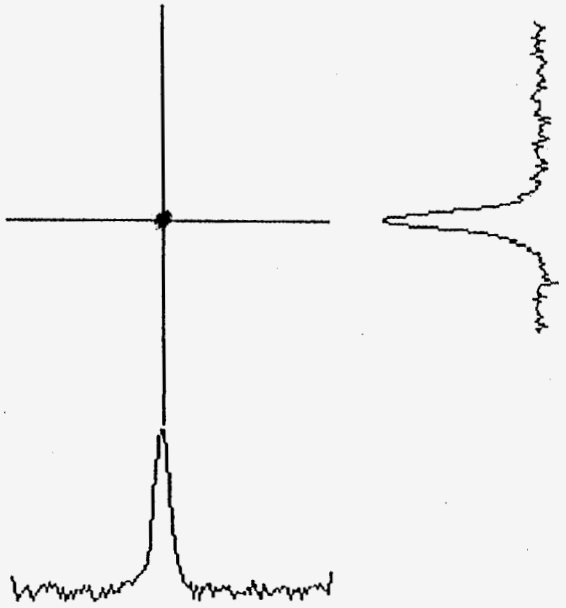

Seeded idler profile
at focus of 500 mm lens
for hemispherical cavity.

Figure 9 / Webb

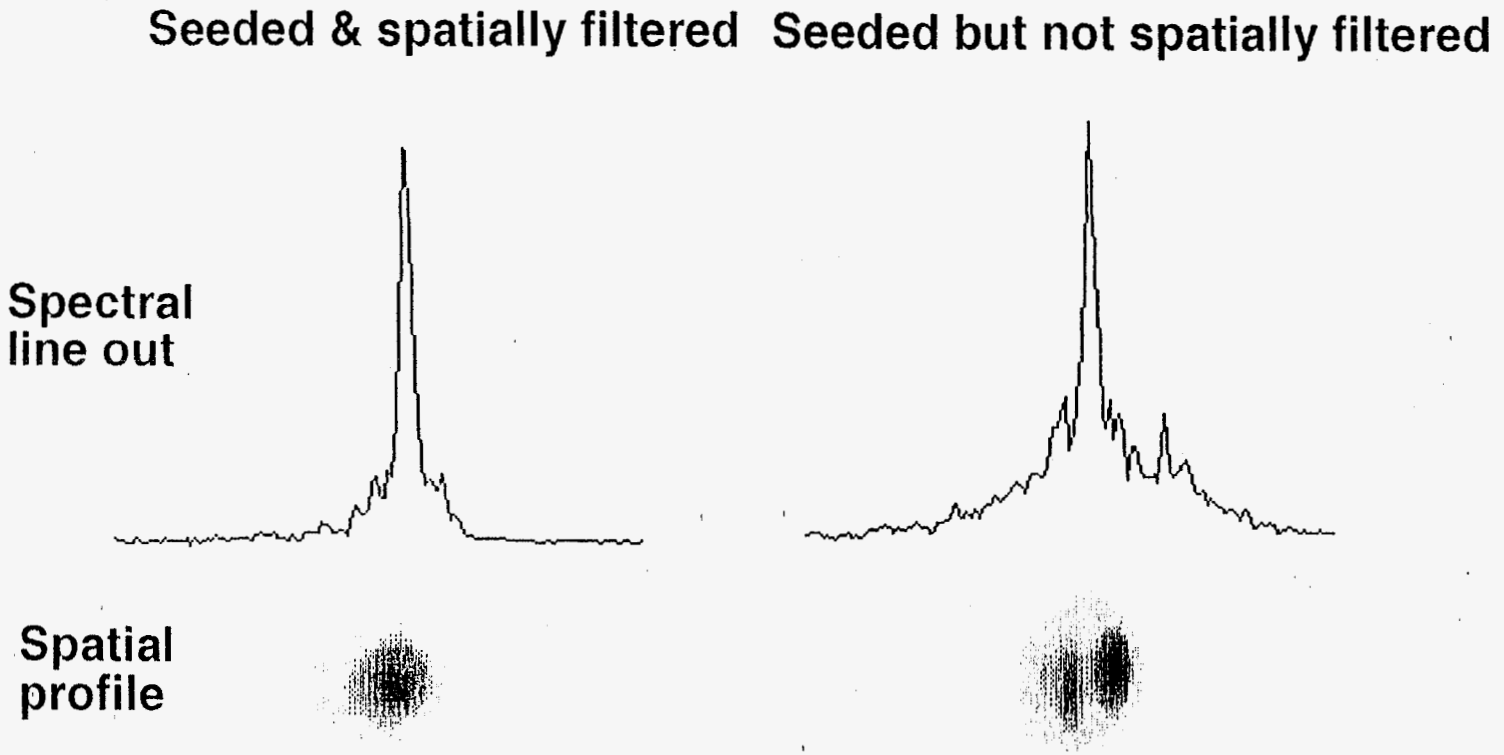

Figure 10 / Webb

Figure 11 / Webb

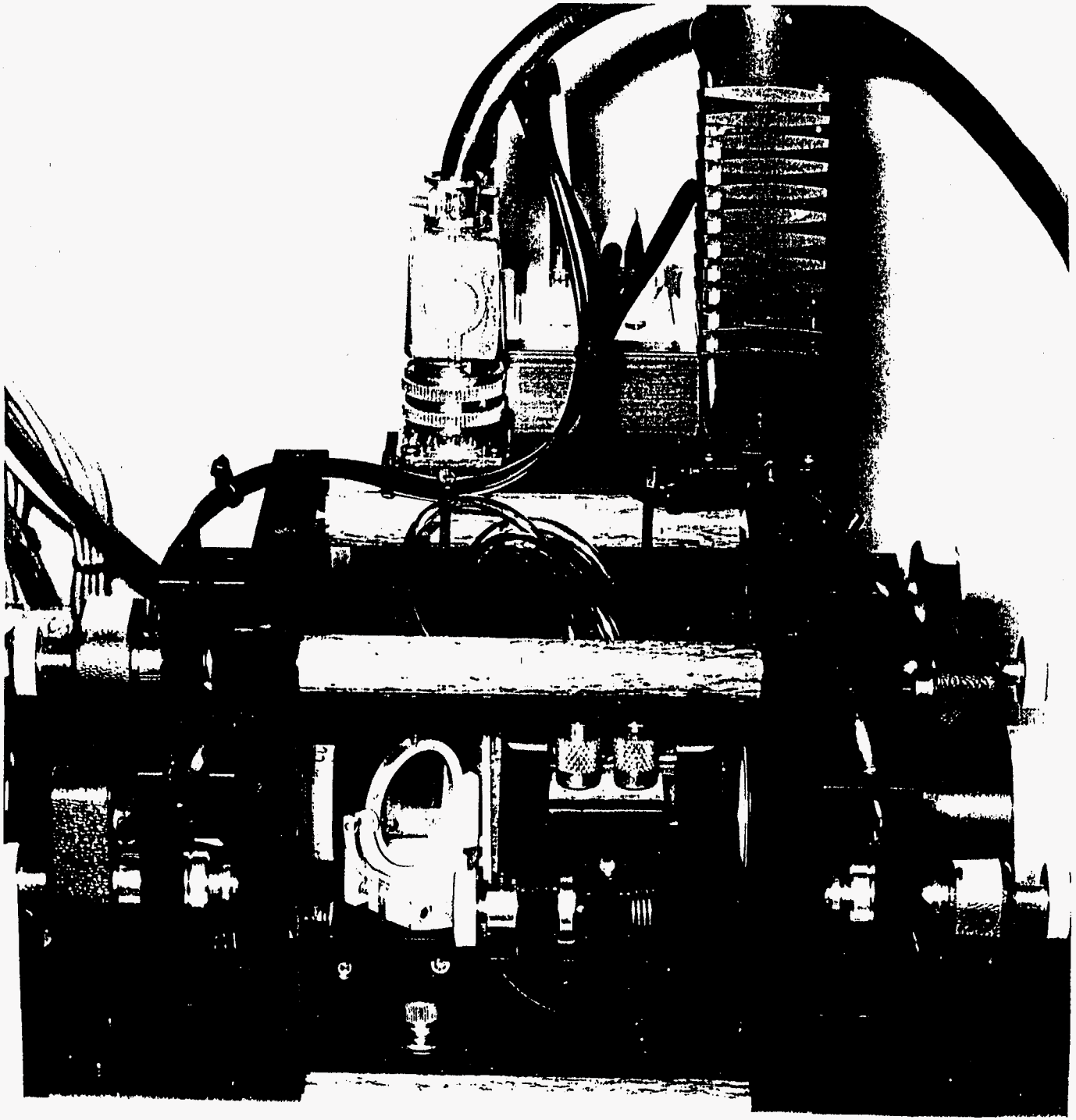

FIG 12 / [illegible]

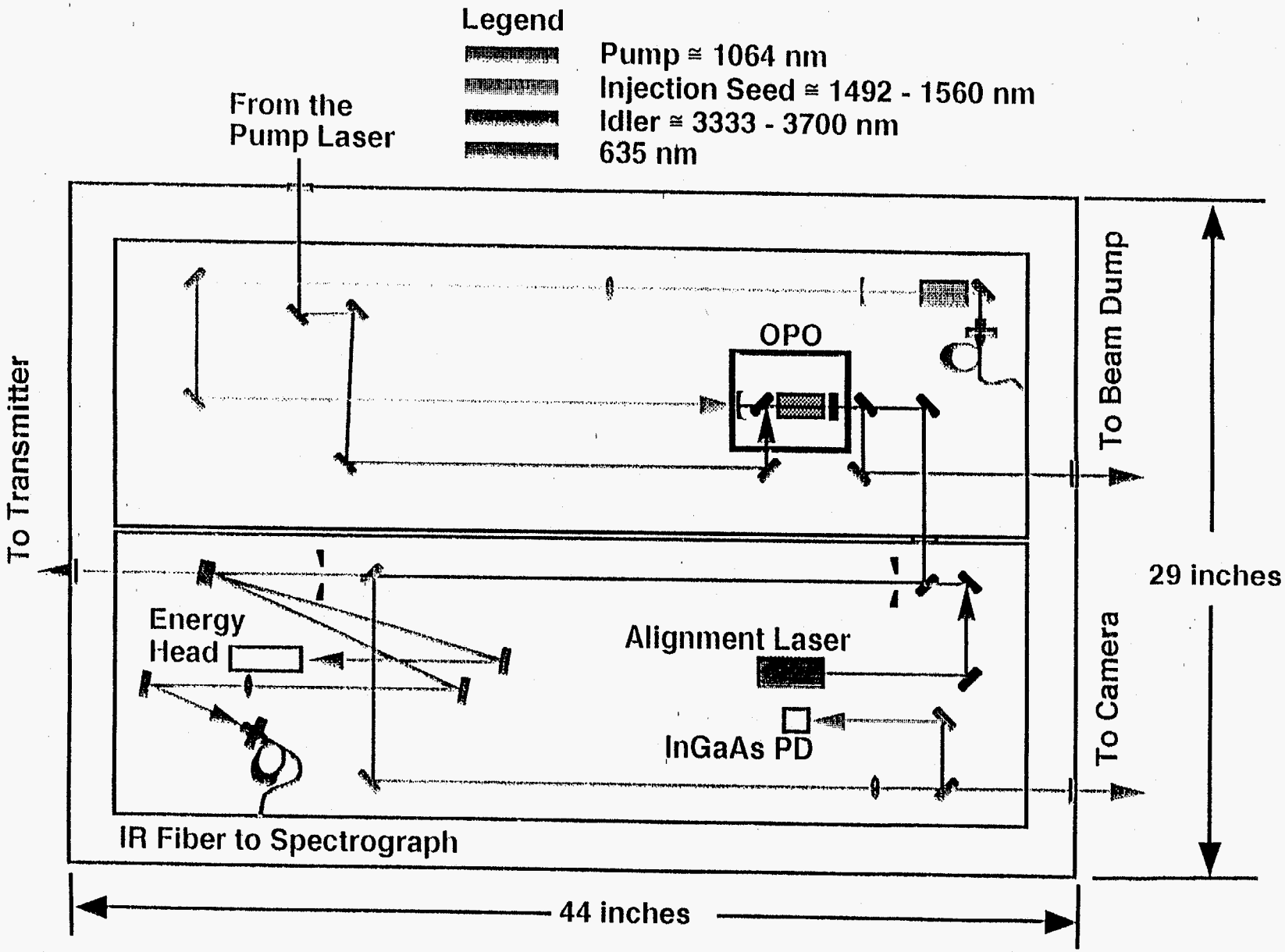

Figure 13 / Webb

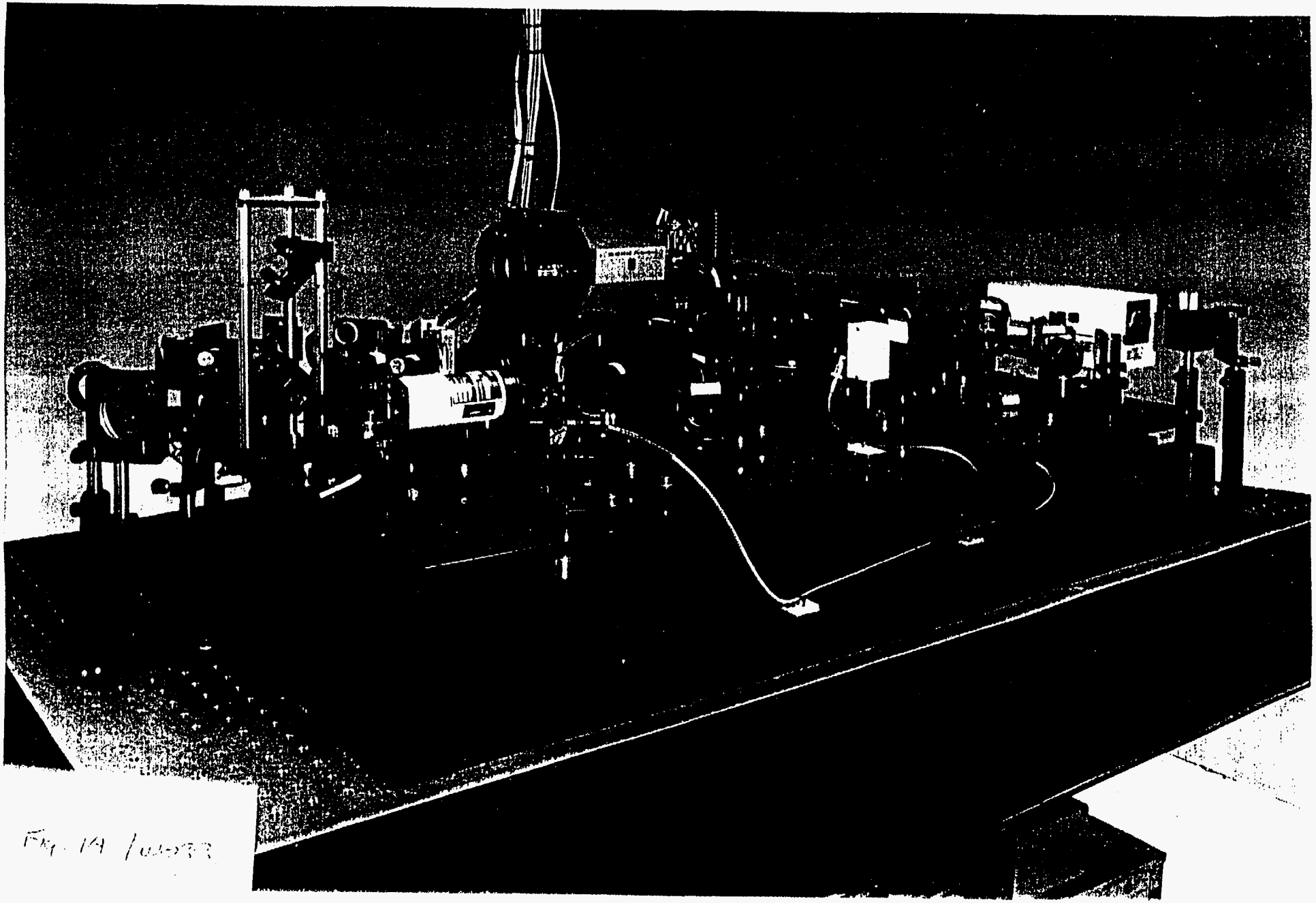

Fig. 14 (illegible)

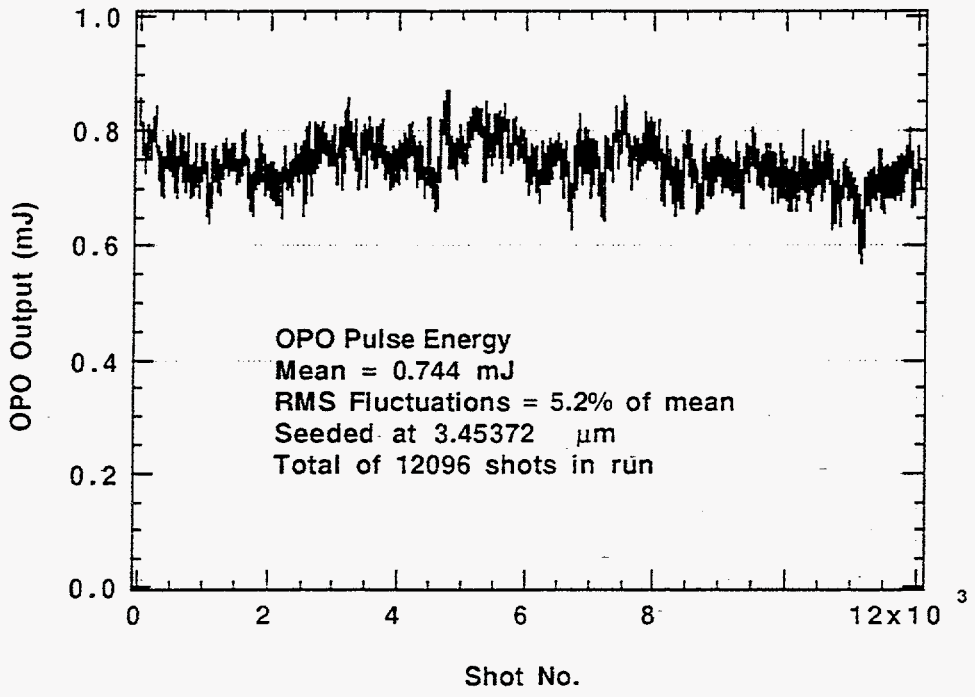

Figure 15 / Webb

Figure 16 / Webb

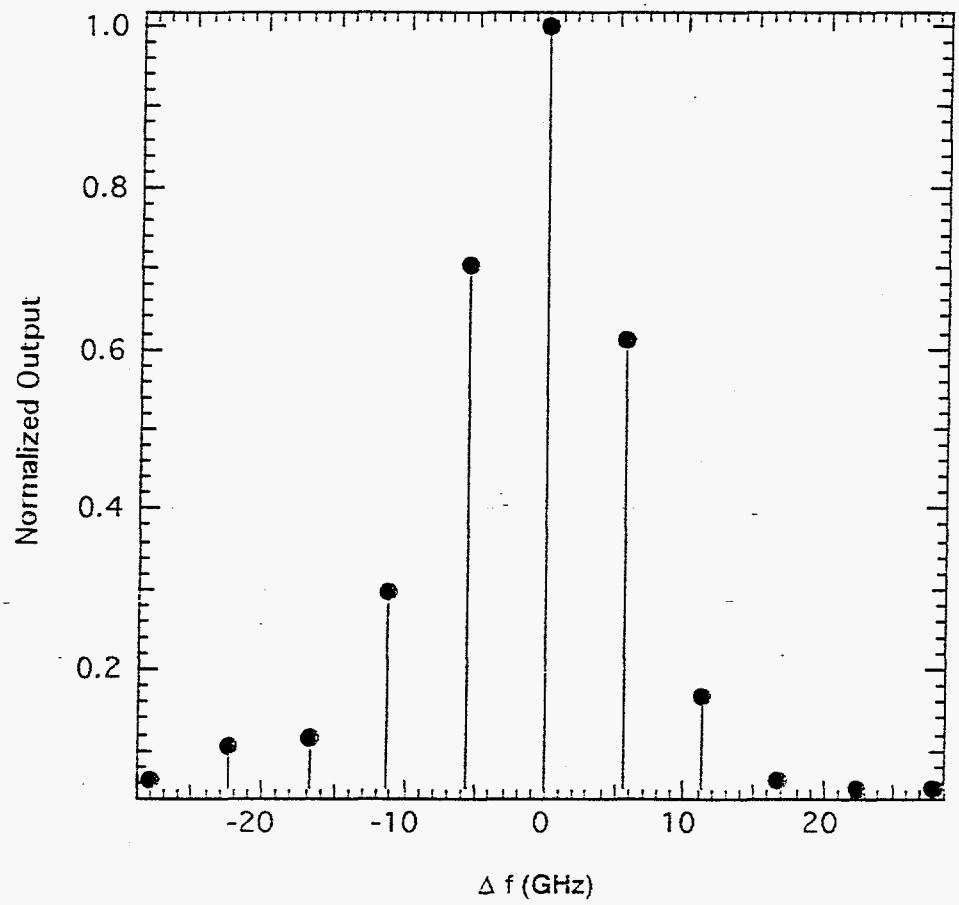

Figure 17 / Webb

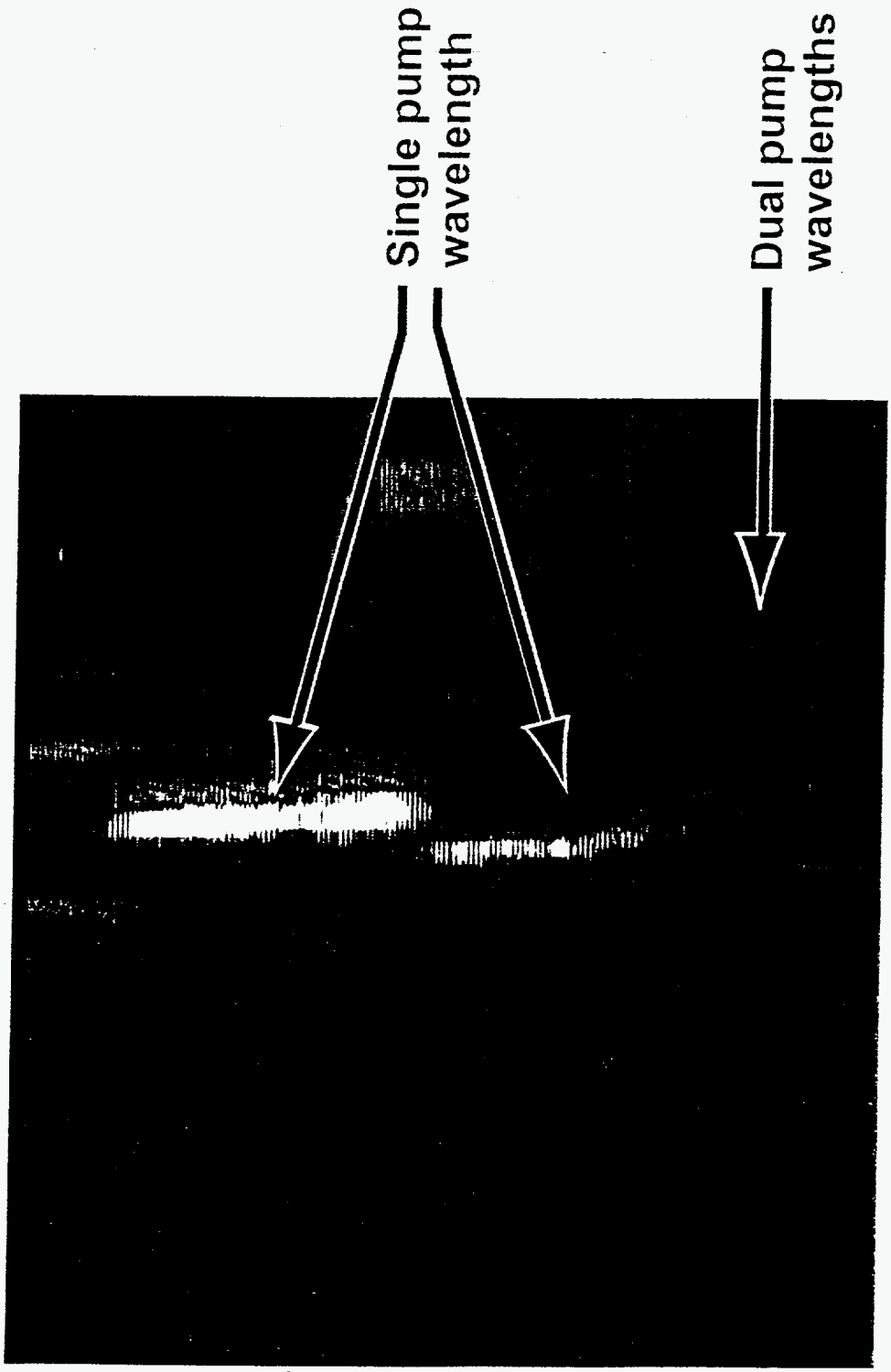

Figure 18/Webb

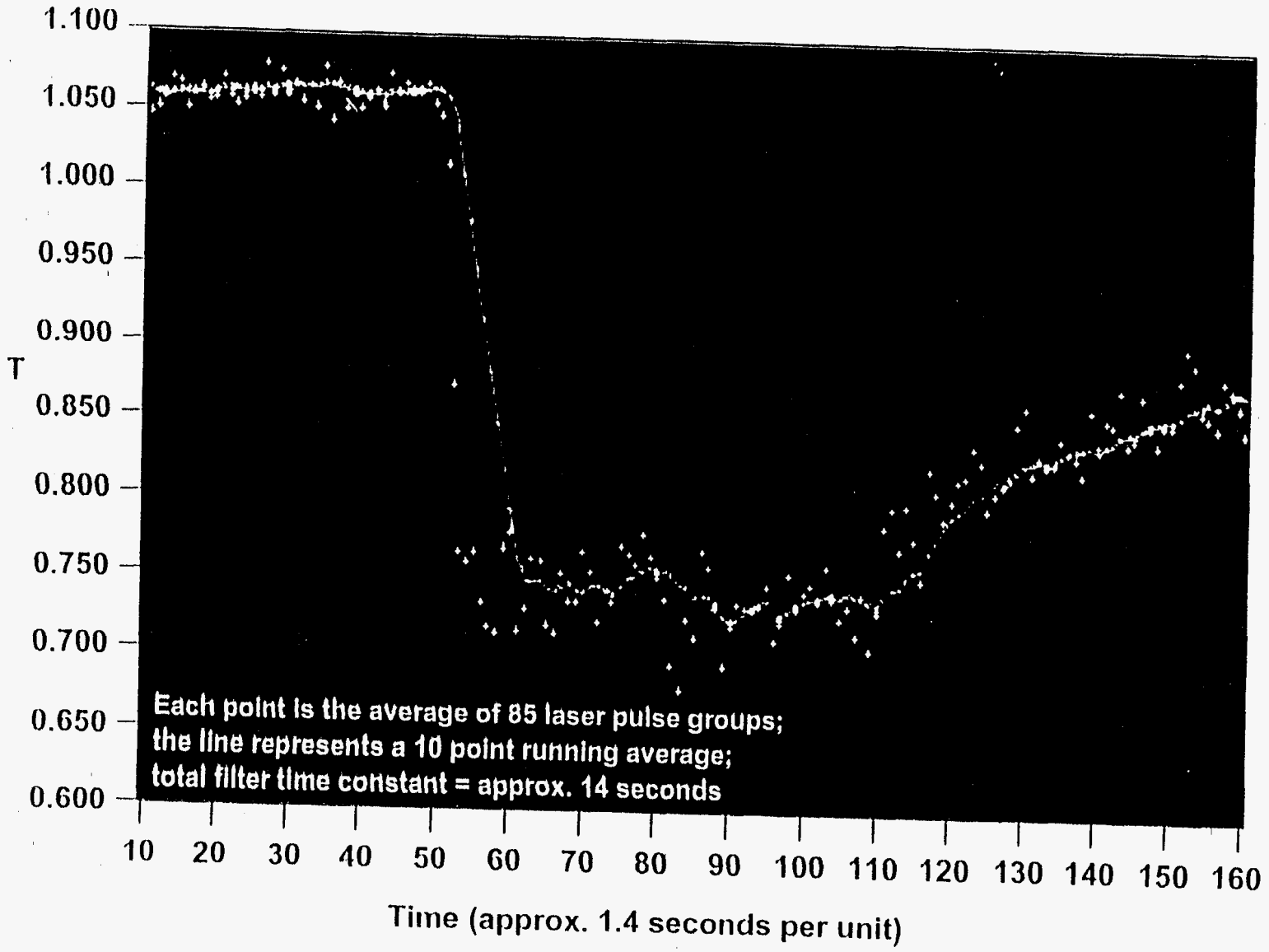

Figure 19/Webb

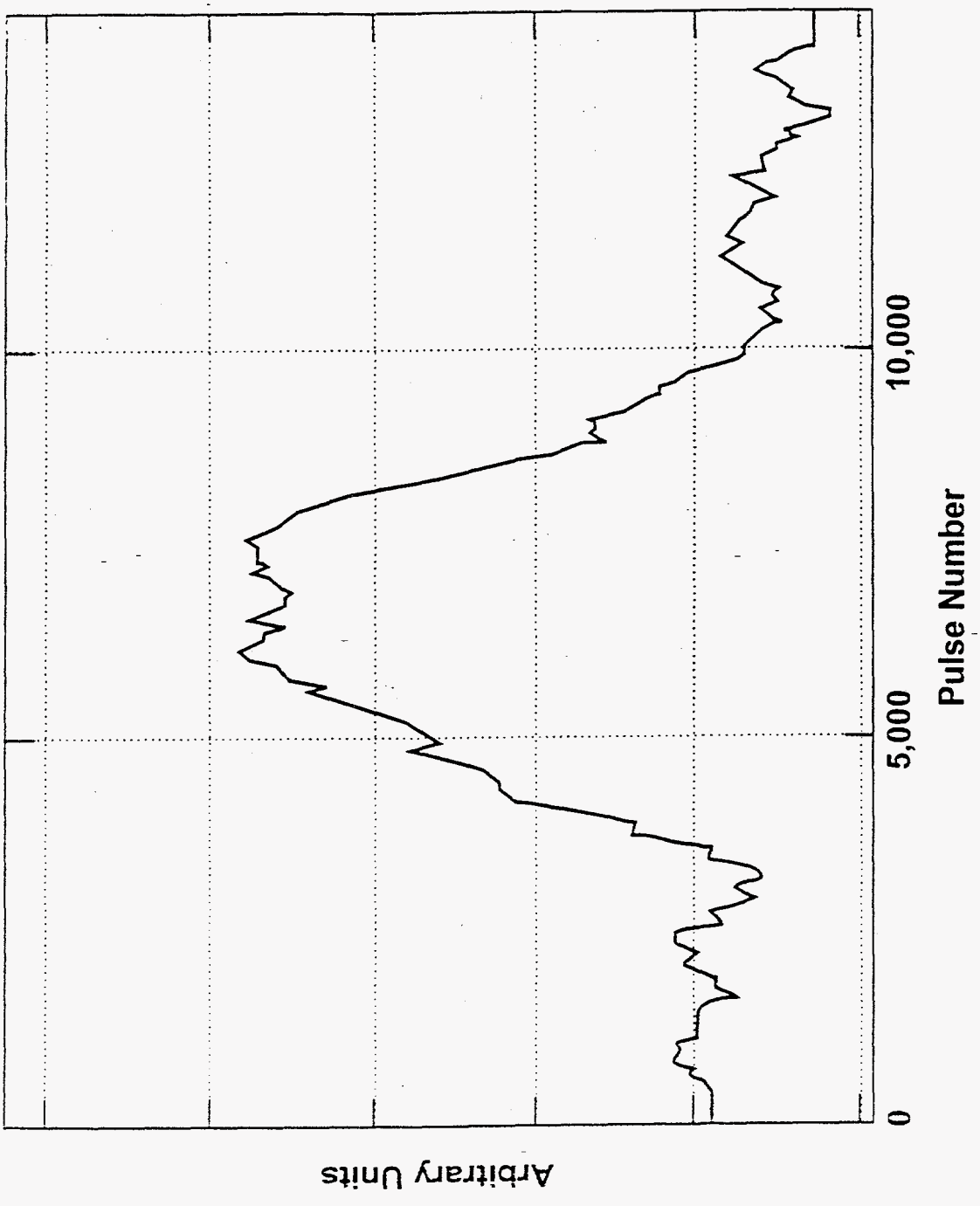

Figure 20/Webb

Author Correspondence:

Mark S. Webb
Lawrence Livermore National Laboratory, L-249
7000 East Ave.
Livermore, CA 94550
Voice: 510-422-8171
Fax: 510-422-3361
e-mail: webb4@llnl.gov

Kenneth B. Stanion
Lawrence Livermore National Laboratory, L-249
7000 East Ave.
Livermore, CA 94550
Voice: 510-422-9695
Fax: 510-422-3361
e-mail: n/a

David J. Deane
Lawrence Livermore National Laboratory, L-476
7000 East Ave.
Livermore, CA 94550
Voice: 510-422-1080
Fax: 510-422-3361
e-mail: n/a

William A. Cook
Lawrence Livermore National Laboratory, L-249
7000 East Ave.
Livermore, CA 94550
Voice: 510-422-8171
Fax: 510-422-3361
e-mail: n/a

William A. Neuman
Lawrence Livermore National Laboratory, L-493
7000 East Ave.
Livermore, CA 94550
Voice: 510-423-8171
Fax:n/a
e-mail: wan@wiley.llnl.gov

Stephan P. Velsko
Lawrence Livermore National Laboratory, L-495
7000 East Ave.
Livermore, CA 94550
Voice: 510-423-0191
Fax: 510-422-3361
e-mail: velsko2@llnl.gov